

SUPERHUMPS IN CATAclysmic Binaries.

XIX. DV URSAE MAJORIS

JOSEPH PATTERSON,¹ TONNY VANMUNSTER,² DAVID R. SKILLMAN,³

LASSE JENSEN,⁴ JOHN STULL,⁵ BRIAN MARTIN,⁶ LEWIS M. COOK,⁷

JONATHAN KEMP,^{1,8,9} AND CHRISTIAN KNIGGE^{1,10}

submitted • *Publications of the Astronomical Society of the Pacific* • 2000 May 10

2000 August 12 Revision

¹ Department of Astronomy, Columbia University, 550 West 120th Street, New York, NY 10027; jop@astro.columbia.edu, christian@astro.columbia.edu

² Center for Backyard Astrophysics (Belgium), Walhostraat 1A, B-3401 Landen, Belgium; tonny.vanmunster@advalvas.be

³ Center for Backyard Astrophysics (East), 9517 Washington Avenue, Laurel, MD 20723; dskillman@home.com

⁴ Center for Backyard Astrophysics (Denmark), Søndervej 38, DK-8350 Hundslund, Denmark; teist@image.dk

⁵ Center for Backyard Astrophysics (Alfred), Division of Physical Sciences, Alfred University, 1 Saxon Drive, Alfred, NY 14802; stulljl@alfred.edu

⁶ Center for Backyard Astrophysics (Alberta), Department of Physics, King's University College, 9125 50th Street, Edmonton, AB T5H 2M1, Canada; bmartin@kingsu.ab.ca

⁷ Center for Backyard Astrophysics (California), 1730 Helix Court, Concord, CA 94518; lcoo@yahoo.com

⁸ Visiting Astronomer, Kitt Peak National Observatory, National Optical Astronomy Observatories, which is operated by the Association of Universities for Research in Astronomy, Inc. (AURA) under cooperative agreement with the National Science Foundation

⁹ Currently at: Joint Astronomy Centre, University Park, 660 North A`ohōkū Place, Hilo, HI 96720; j.kemp@jach.hawaii.edu

¹⁰ Hubble Fellow

ABSTRACT

DV Ursae Majoris is a deeply eclipsing dwarf nova which shows very powerful superhumps when it attains superoutburst. We report detailed observations of the 1997 and 1999 eruptions. Some of the results reproduce what has been learned from other eclipsing dwarf novae: that the disk becomes very large in outburst; that superhumps develop in a few days; that superhumps remain strong even after the disk has shrunk by $>30\%$. The mean superhump period was $0.08870(8)$ d, but in both eruptions the period decreased with $\dot{P} \approx -6 \times 10^{-5}$. Globally distributed coverage of the 1997 eruption revealed two other interesting features: a transient strong modulation at the *orbital* period at the peak of eruption, and intricate fine structure in the harmonics of the main superhump signal. In particular, we found that the second harmonic occurred not at $3\omega - 3\Omega$ as expected (where ω and Ω are respectively the orbital and “precession” frequencies), but at $3\omega - 2\Omega$ and $3\omega - \Omega$. The strong orbital modulation may have arisen from enhanced mass transfer from the secondary.

We also report photometry at quiescence, which separates the luminous contributions of the white dwarf, accretion disk, and secondary star. We estimate a distance of 350 ± 120 pc. Analysis of the eclipses suggests $i = 84.0 \pm 0.8^\circ$, $q = 0.155 \pm 0.015$, $M_2 = 0.14 \pm 0.02 M_\odot$, $M_1 = 0.90 \pm 0.13 M_\odot$.

Subject headings: accretion, accretion disks — binaries: close — novae, cataclysmic variables — stars: individual (DV Ursae Majoris)

1. INTRODUCTION

DV Ursae Majoris was discovered by Usher et al. (1982) in a search for ultraviolet-excess objects, and then identified as an eclipsing cataclysmic variable by Howell et al. (1988). The CV identification along with the brightness variations noted by Usher et al. (magnitude 15–20) suggested that the star is probably a dwarf nova. Deep eclipses during outburst were noted by Nogami (1995) and Vanmunster (1997).

Extensive visual observation since 1995 has established that the star is a dwarf nova of the SU Ursae Majoris type. Because eclipses offer great diagnostic power in revealing the structure of the binary, we have placed high priority on time-series photometry of DV UMa. The 1995 outburst was known to be short (“normal”), while the 1997 and 1999 outbursts (“super”, spaced by 2.7 years) were long. We obtained coverage of the two superoutbursts, as well as photometry at quiescence. We report the details here.

2. OBSERVATIONS

Most of the observations reported here consist of differential CCD photometry on the globally distributed telescopes of the Center for Backyard Astrophysics (CBA, Skillman & Patterson 1993). These telescopes range from 0.25 to 0.81 m in aperture, and the cameras typically use the Kodak KAF-0400 chip, operating unfiltered and therefore sensitive to 5000–9000 Å light. For a blue star like a cataclysmic variable, this gives an effective wavelength near 6300 Å. In our usual technique, we declare a “campaign” on a particular target star, and collect light curves which overlap sufficiently in time to permit calibration of the instrumental delta-magnitudes. That calibration is typically accurate to ~0.05 mag (0.02 mag on a given night, but small differences exist from night to night). Some data are also obtained through standard *BVRI* filters to put the light curves on an “absolute” *V* scale. That calibration is no better than 0.1 mag, or even as coarse as 0.25 mag if the star's colors change drastically (e.g., between outburst and quiescence).

Some additional outburst photometry was obtained with an unfiltered CCD on the KPNO 0.91 m telescope. The observations at quiescence were obtained with the MDM 1.3 m and 2.4 m telescopes, using *UBVRI* and Schott *BG38* (giving a “broad blue” bandpass) filters. The log of observations during 1997–2000 is presented in Table 1, comprising 231 hr over 55 nights.

3. ORBITAL EPHEMERIS AND QUIESCENT LIGHT CURVE

The star's deep eclipses make it easy to measure times of mid-eclipse, which we present in Table 2. We made a linear fit to these, along with a few other timings previously published or extracted from published light curves, and found the following orbital ephemeris:

$$\text{Minimum light} = \text{HJD } 2,446,854.8336(3) + 0.08585265(1)E. \quad (1)$$

Figure 1 is an O–C diagram of the minima with respect to this ephemeris. There may be some systematics in the scatter about the best fit, arising from differences between quiescence

and outburst, ways of defining minimum light, or even actual (small) period changes. But these subtleties are mostly lost in the noise of the data, and we adopt this as a satisfactory long-term ephemeris for minimum light. We shall find below that the centroid of the white-dwarf eclipse is slightly displaced from minimum light (by -58 ± 15 s); this will result in an alternative (and superior, since the white dwarf mid-eclipse is an event of dynamical significance) ephemeris in §7.1. We used the latter for all phases quoted in this paper.

A long light curve in the quiescent state is shown in the upper left frame of Figure 2, revealing the basic shape: a deep, slightly asymmetric eclipse superimposed on a very asymmetric double-humped variation. The lower frames of Figure 2 show the folded light curve in B , V , and I light. The I light curve is dominated by the double-humped variation, the signature of a tidally distorted secondary. The B light curve shows a sharp and very deep eclipse, indicating that the light is dominated by a small light source centered on the white dwarf. All light curves in quiescence show the prominent hot spot at orbital phase 0.81 ± 0.02 .

On several nights we increased the time resolution through eclipse, to try to resolve the eclipse structure. On one night, seeing and transparency stayed good through two consecutive orbits, and the upper right frame of Figure 2 shows the result of superposing those orbits. The eclipse structure was found to closely resemble that of other deeply eclipsing dwarf novae in quiescence, with the light dominated by the white dwarf and hot spot (e.g. see Figure 2 of Wood et al. 1989a). The first rapid drop is centered at phase 0.9684 and takes 44 ± 22 s; this is ingress of the white dwarf. The second drop occurs at phase 0.9920 and takes 135 ± 50 s; this is ingress of the hot spot. Minimum light occurs at phase 0.0103. The first recovery occurs at phase 0.0315 and takes 28 ± 12 s; this is egress of the white dwarf. The final rise occurs at phase 0.0711 and takes < 35 s; this is egress of the hot spot. All these phases refer to mid-ingress and -egress, and are based on a weighted average over all data. The duration of the white-dwarf eclipse is 467 ± 8 s.

We can use these light curves (in particular, the well-separated I and B curves which are plainly dominated by different components, and the eclipse shape which marks the brightness and size of the components) to deconvolve the various light sources. We adopt 0.32 mag as the estimated true amplitude of tidal distortion at the relevant mass ratio (Bochkarev, Karitskaya, & Shakura 1979). In B light, the apparent magnitudes are: white dwarf, $B=19.9 \pm 0.2$; red star, $B > 21.5$; other light, $B=19.3 \pm 0.1$. In I light, these magnitudes are respectively > 19.6 , 18.0 ± 0.1 , and 19.3 ± 0.2 . These magnitudes are orbit-averaged, and are consistent with the fractional contribution of the secondary implied by the spectrum (Mukai et al. 1990).

These provide preliminary estimates of the distance to DV UMa. With the secondary's spectral type estimated as $M4.5 \pm 0.5$ (Mukai et al. 1990), the main-sequence M_I -spectral type relation of Bessell (1998) yields $M_I=10.0-11.3$ and hence a distance of 220–400 pc. The other useful distance constraint comes from the known correlation between P_{orb} and M_V at the peak of a normal eruption (Vogt 1981, Warner 1987). DV UMa has an estimated $V(\text{max})=15.1 \pm 0.3$, but at its likely inclination of $i=84^\circ$ the disk light is diminished by ~ 2.2 mag relative to the “standard inclination” of $i=56^\circ$ (Mayo et al. 1980, Warner 1995). Allowing an additional uncertainty of 0.7 mag for the inclination correction, we adopt a corrected $V(\text{max})=12.9 \pm 0.9$. The empirical

correlation predicts $(M_v)_{\max}=5.1\pm 0.3$ at $P_{\text{orb}}=2.06$ hr, so we obtain a distance of 240–540 pc. Both estimates are consistent with 350 ± 120 pc.

4. THE 1997 SUPEROUTBURST

DV UMa was reported at magnitude 14.0 by T. Kinnunen and T. Vanmunster (vsnet-alert 828, 830) on 1997 April 8.9, certifiably the first night of eruption (upper limits were obtained by Vanmunster and G. Poyner the previous night). We began time-series photometry the next night, and amassed 130 hours of coverage over 18 nights in the 20-night eruption. Orbit-averaged magnitudes are recorded in Table 1, and shown in the eruption light curve of Figure 3.

Selected long light curves are shown in Figure 4. Deep eclipses are seen throughout, plus a smooth wave which migrates in orbital phase, surely the “superhump” which distinguishes all SU UMa stars in superoutburst (reviewed in Chapter 3.6 of Warner 1995).

After removing the eclipses we calculated the amplitude spectrum of the seven-night light curve (truncated JD 549–555) from the discrete Fourier transform. The result is shown in the lower frame of Figure 5. The main signal obeys the ephemeris

$$\text{Maximum light} = \text{HJD } 2,450,549.4012 + 0.08880(6) E, \quad (2)$$

during this interval, with the mean waveform shown in the inset. The amplitude spectrum proved to be quite interesting. Because the light curves span a very wide range of terrestrial longitude, there was no difficulty with daily aliasing, so it was easy to identify the correct frequencies and then “clean” the unwanted aliasing pattern of the strongest signals from the amplitude spectrum. Six significant detections were found, labelled in Figure 5 with their frequencies in c/day.

Superhump maxima were quite well defined, so we timed them carefully and used the data (collected in Table 3) to look for period changes over the full time span via the O–C diagram in the lower left frame of Figure 6. The result is somewhat confusing, because the first night (and to some extent the second) is very discrepant. All other timings are satisfactorily fit with an ephemeris shown by the curve in Figure 6:

$$T_{\max} = \text{HJD } 2,450,548.455 + 0.08906 E - 2.48 \times 10^{-6} E^2. \quad (3)$$

The quadratic term corresponds to $\dot{P} = -5.6(\pm 1.4) \times 10^{-5}$, a typical value for dwarf novae.

We could not plausibly account for the first night's timings by any simple adjustment to cycle count. A power spectrum of the first two nights only explains why, and is shown in the upper frame of Figure 6. The two signals detected are consistent with the fundamental and first harmonic of the *orbital* frequency, not that of the superhump. This is also suggested by the severe downward slope in the O–C during $E=0-13$. A fold of the first night's data alone on P_{orb} yielded the mean light curve shown in the lower right frame of Figure 6. Humps occur at phase

0.5 and (probably) 1.0, with the usual deep eclipse superimposed.

5. THE 1999 SUPEROURBURST

DV UMa was discovered again in superoutburst on 1999 December 8.20 by T. Kinnunen (vsnet-obs 25179), and we conducted another campaign during December 10–20. The light curves obtained were similar to those of Figure 4, but our coverage, detailed in Table 1, was more sparse. Aliasing difficulties (not 24-hour aliases, but more subtle ones) made the process of “cleaning” the power spectrum complicated and non-unique, so we present only the raw power spectrum in the lower frame of Figure 7, along with the mean waveform. The mean frequency was 11.29 ± 0.01 c/day ($P=0.0886$ d), with a weak first harmonic.

The upper frame of Figure 7 presents other data on the 1999 eruption. At left is the V light curve, based on the data in Table 1 and the VS-NET collection. Comparison with Figure 4 shows that the 1999 eruption was 0.5 mag fainter, with the same duration (17 ± 2 d) and decline rate (0.10 ± 0.01 mag/d). The right panel is an O–C diagram of the timings of superhump maximum. The timings acceptably follow the ephemeris

$$T_{\max} = \text{HJD } 2,451,523.446 + 0.08904 E - 4.01 \times 10^{-6} E^2, \quad (4)$$

indicating period decrease at a rate $\dot{P} = -9(\pm 4) \times 10^{-5}$. This period decrease is consistent with the (probably) better-determined value found in the 1997 eruption (Figure 6).

6. SUPERHUMPS

6.1 *The Common Superhumps*

Roughly speaking, the superhumps of DV UMa follow all the usual rules for this phenomenon: they develop within 2–3 days of eruption onset; they show a period excess of 3.3% over P_{orb} ; they show a slow period decrease with $\dot{P} \approx -6 \times 10^{-5}$. They are basically textbook *common superhumps*. But some of the details described above call for more discussion.

6.2 *(Quasi-)Harmonics*

The frequencies marked in Figure 5 deserve close inspection. Very roughly, these are the “harmonics” of the main signal. But several do not occur at strict multiples of the fundamental frequency, and hence are not exactly harmonics. More exactly, let us label the orbital frequency as ω and the main superhump as $\omega - \Omega$, where Ω is the frequency of precession; this is the “apsidal precession” theory (Whitehurst 1988) which has now become the standard theory of common superhumps. In this case, $\omega = 11.648$ and $\Omega = 0.39$ c/day. The six labelled signals in Figure 5 are then $\omega - \Omega$, $2(\omega - \Omega)$, 2ω , $3\omega - 2\Omega$, $3\omega - \Omega$, and $4(\omega - \Omega)$. The simple integer multiples of $\omega - \Omega$ are not surprising; they presumably signify only a nonsinusoidal superhump waveform. The signal at 2ω is also not surprising, since we identify a stronger orbital signal in the first 1–3 days of eruption. The detection of $3\omega - 2\Omega$ and $3\omega - \Omega$ is surprising, however; such features are quite rarely seen (IY UMa is the only published example) in the light curves of dwarf novae.

But they have been clearly seen in superhumping novalike variables, especially in AM CVn where at least ten signals of this type have been detected (Provencal et al. 1995, Skillman et al. 1999). In AM CVn a simple rule relates the many frequencies: they are of the form $n\omega - m\Omega$, where n is any integer and $m=1, 2, \dots, n$. DV UMa conforms to this. It is a plausible speculation that more sensitive searches in dwarf novae may yield similar results (the searches in AM CVn are 5–10 times more sensitive than any search in a dwarf nova).

6.3 *The Outburst Orbital Hump*

The orbital modulation at the start of the 1997 eruption is certainly an interesting feature. A 0.25 mag modulation at $V=14.1$ represents a factor of 30 enhancement over the orbital flux modulation in quiescence. These are quite unusual features in dwarf novae. At the suggestion of an anonymous referee a few years ago, we call them “outburst orbital humps” (to distinguish from superhumps, where $P \neq P_{\text{orb}}$). There appear to be only three documented detections published so far: in WZ Sge (Patterson et al. 1981), AL Com (Patterson et al. 1996, Nogami et al. 1997), and EG Cnc (Patterson et al. 1998). Another good candidate is HV Vir (Leibowitz et al. 1994). The origin of such signals remains unknown. Interestingly, all are stars of very long recurrence time, which represent only $\sim 15\%$ of dwarf novae with well-studied superhumps. Such statistics hint that superoutbursts in these “WZ Sge stars” may have a somewhat different origin. In particular, these signals could arise from a hot spot transiently enhanced by a burst of mass transfer from the secondary. The reasons for favoring this, discussed in the above-mentioned papers, might be worth another peek.

7. ECLIPSE ANALYSIS

7.1 *Quiescence*

Our best light curves in quiescence were of sufficient quality to permit deconvolution of the eclipsed light into its major components (white dwarf, hot spot, and disk proper). And they permitted timings of eclipse phases, which furnished constraints on binary parameters. Eclipse measurements of sufficient quality are given in Table 4, where we have adopted the terminology

t_{wdi}	=	white dwarf mid-ingress
t_{hsi}	=	hot-spot mid-ingress
t_{min}	=	minimum light
t_{wde}	=	white dwarf mid-egress
t_{hse}	=	hot-spot mid-egress

Most of the measurements were straightforward, except for the *durations* of white-dwarf ingress and egress. The star is too faint to permit accurate measurement of this brief interval, and most of the eclipses gave only upper limits. A few runs gave marginally significant measurements (rather than limits) for egress; and from the totality of data we estimate that the duration is 30 ± 8 s.

The times of white-dwarf mid-ingress and mid-egress are stable, as is their difference (467 ± 8 s). The average of these times defines mid-eclipse (superior conjunction of the white dwarf), which follows the ephemeris

$$\text{White dwarf mid-eclipse} = \text{HJD } 2,451,216.92041(6) + 0.08585265(1) E. \quad (5)$$

We actually used this phase convention for the subsequent eclipse analysis, since mid-eclipse is the event of dynamical significance.

It is possible to constrain q accurately by using the timings of white-dwarf and hot-spot eclipses. We used the method of Wood et al. 1989a (see also Smak 1971, Smak 1979, Cook & Warner 1984, Ritter & Schroeder 1979) and found the result shown in Figure 8. We used the average binary phases from the 1999 and 2000 data separately. The former was obtained long after outburst, and might thus be considered more reliable (issues of disk ellipticity are worrisome for data obtained very close to superoutburst). On the other hand, the 2000 data were of substantially better quality. Perhaps it is best to accord equal weight and consider the disagreement in q to be a measure of the uncertainty. We estimate $q=0.155 \pm 0.015$.

Figure 9 combines this constraint with two other available constraints: the $q(i)$ relation from the eclipse duration, and the ingress/egress duration. For the latter we used the Nauenberg (1972) mass-radius relation for the white dwarf. The hard limit at $i=90^\circ$ is also shown.

Finally, there is some information directly available about the secondary, independent of the white dwarf. The observed spectral type of $M4.5 \pm 0.5$ (Mukai et al. 1990) implies an effective temperature $T_{\text{eff}}=3040 \pm 120$ deg, which implies $M_2=0.13\text{--}0.18 M_\odot$ from models of main-sequence stars of solar metallicity (Chabrier & Baraffe 1995), or $M_2=0.12\text{--}0.17 M_\odot$ from observations of the same (Henry et al. 1999). Thus the main-sequence assumption requires $M_2=0.12\text{--}0.18 M_\odot$. This is unlikely to be far wrong, since we earlier found approximate agreement between distances inferred from the main-sequence assumption and from the empirical $P_{\text{orb}}\text{--}M_v(\text{max})$ relation for dwarf novae.

Points in the black region of Figure 9 satisfy all constraints. In summary, our eclipse analysis favors $i=84.0 \pm 0.8^\circ$, $q=0.155 \pm 0.015$, $M_1=0.90 \pm 0.13 M_\odot$, and $M_2=0.15 \pm 0.02 M_\odot$.

7.2 Outburst

During superoutburst, the eclipse is broad and smooth, and we measured primarily two quantities: total eclipse width (first to last contact) and time of minimum light. The latter is given in Table 2. The eclipse widths were particularly well-sampled in the 1997 eruption, and we present these data in the lower frame of Figure 10 (along with a representative error for the measurements of total widths, subject to the caveat described below). Figure 10 shows that eclipses at the peak of eruption were nearly twice as long as they were at quiescence.

The reason for this is certainly that the disk is much larger at the peak of eruption, as has been found for several other stars (O'Donoghue 1986, Zola 1989, Smak 1984, Wood et al.

1989b) — and as expected for dwarf novae in general. For the binary parameters favored above, solution of Kepler's Third Law gives a simple approximation for disk radius as a function of eclipse width W :

$$R_d/a = -0.20 + 3.17 W, \quad (6)$$

which yields the disk radii shown by the inset scale in Figure 10.

So the *prima facie* conclusion is that the radius contracted by at least 30%. The actual values of R_d/a are interesting too. The critical radius for sustenance of superhumps is $0.46a$, where the disk's 3:1 orbital resonance occurs. The disk appears to contract within this radius by JD 553 ± 1 d. But the observed evolution of superhump amplitude is shown in the upper frame, and shows no sharp dependence on the shrinkage of the disk.

Since the “disk radius” is here considered from photometric evidence only, it is in principle possible that the eclipse of light emitted at large radius is simply too difficult to spot amid the noise of flickering. This must be true in quiescence, because it is then sometimes difficult to see any decline in light until the white dwarf itself is eclipsed; the trailing lune of the disk must exist, but is invisible. After JD 560, it's a significant worry, since the disk is then quite faint; those late measurements should be accorded much lower weight. But the disk dominates the light until JD 560, so it appears that the simplest interpretation of Figure 10 is correct: superhumps endured for >5 days after the resonant condition was no longer satisfied.

Probably the reason for this is that the superhump does not come from a strictly local heating of the outer disk slavishly tied to alignments of the secondary with the disk's apses. It is more properly a global oscillation of the disk (at least a large portion of it) originally excited by a resonant condition near the outer edge. This important point is stressed and illustrated by Simpson & Wood (1998). Empirical evidence suggests that superhumps outlast the resonant conditions for at least a few dozen binary orbits.

8. SUMMARY

1. We present photometry of the 1997 and 1999 superoutbursts, which show common superhumps with $P=0.08870(8)$ d, slowly changing with $\dot{P} \approx -6 \times 10^{-5}$. The superhump harmonics showed complex sidebands, consistent with the description “ $n\omega - m\Omega$ ” (detections at $3\omega - \Omega$ and $3\omega - 2\Omega$, as well as simple harmonics).
2. The first two photometry nights (excluding the very first night of eruption, when no photometry was obtained) of the 1997 eruption showed powerful waves at the orbital frequency and its first harmonic. The origin of such “outburst orbital humps” is still unknown, and a matter of importance since it may be intimately involved with the cause of the superoutburst. It is possible that they arise from a brilliant hot spot, intensified by a burst of mass transfer from the secondary.
3. Multicolor photometry in quiescence resolves the photometric contributions of the various

components in the binary. As usual in eclipsing dwarf novae of short P_{orb} , the blue light is dominated by the white dwarf and the hot spot at disk's edge. In I light the tidally deformed secondary is dominant. Two distance estimators converge on 350 ± 120 pc.

4. High-speed photometry in eclipse reveals the sizes and locations of the white dwarf and the hot spot, and a $q(i)$ relation. These supply constraints on the component masses. The black region in Figure 9 satisfies these constraints, with $i=84.0 \pm 0.8^\circ$, $q=0.155 \pm 0.015$, $M_1=0.90 \pm 0.13 M_\odot$, and $M_2=0.15 \pm 0.02 M_\odot$.
5. Measurement of eclipse widths yields the radius of the accretion disk, and the radius became much larger ($\sim 0.5a$) in superoutburst. It appeared to contract quickly to $< 0.33a$, well within the 3:1 orbital resonance, even though the superhumps endured for another ~ 100 binary orbits.

Thanks to all the skilled visual observers, especially Timo Kinnunen, for their great vigilance which enables us to identify these stars and the outbursts we love to study. Thanks also to the Research Corporation (grant GG-0084) and the National Science Foundation (grant AST96-18545) for their generous support of CBA science. Support was provided in part by NASA through Hubble Fellowship grant HF-01109 awarded by the Space Telescope Science Institute, which is operated by the Association of Universities for Research in Astronomy, Inc., for NASA under contract NAS 526555.

REFERENCES

- Bessell, M. S. et al. 1998, *A&A*, 333, 231.
Bochkarev, N.C., Karitskaya, E.A., & Shakura, N.I. 1979, *Astr. Zh.*, 56, 16.
Chabrier, G. & Baraffe, Y. 1997, *A&A*, 327, 1039.
Cook, M.C. & Warner, B. 1984, *MNRAS*, 207, 705.
Henry, T. et al. 1999, *ApJ*, 512, 864.
Howell, S.B., Warnock, A., Mason, K.O., Reichert, G.A., & Kreidl, T.J. 1988, *MNRAS*, 233, 79.
Leibowitz, E., Mendelson, H., Bruch, A., Duerbeck, H.W., Seitter, W.C., & Richter, G.A. 1994, *ApJ*, 421, 771.
Mayo, S., Wickramasinghe, D.T., & Whelan, J.A.J. 1980, *MNRAS*, 193, 793.
Mukai, K. et al. 1990, *MNRAS*, 245, 385.
Nauenberg, M. 1972, *ApJ*, 175, 417.
Nogami, D. 1995, vsnet-alert, 55 (<http://www.kusastro.kyoto-u.ac.jp/vsnet/Mail/vsnet-alert/msg00055.html>).
Nogami, D. et al. 1997, *ApJ*, 490, 840.
O'Donoghue, D. 1986, *MNRAS*, 220, 23p.
Patterson, J., McGraw, J.T., Coleman, L., & Africano, J.L. 1981, *ApJ*, 248, 1067.
Patterson, J. et al. 1996, *PASP*, 108, 748.
Patterson, J. et al. 1998, *PASP*, 110, 1290.
Provencal, J. et al. 1995, *ApJ*, 445, 927.
Ritter, H. & Schroeder, R. 1979, *A&A*, 76, 168.
Simpson, J.C. & Wood, M.A. 1988, *ApJ*, 506, 360.
Skillman, D.R. & Patterson, J. 1993, *ApJ*, 417, 298.
Skillman, D.R. et al. 1999, *PASP*, 111, 1281.
Smak, J.I. 1971, *Acta Astr.*, 21, 15.
Smak, J.I. 1979, *Acta Astr.*, 29, 309.
Smak, J.I. 1984, *Acta Astr.*, 34, 93.
Usher, P.C., Mattson, D., & Warnock, A. 1982, *ApJS*, 48, 51.
Vanmunster, T. 1997, vsnet-alert, 830 (<http://www.kusastro.kyoto-u.ac.jp/vsnet/Mail/vsnet-alert/msg00830.html>).
Vogt, N. 1981, *Mitt. Astr. Gesell.*, 57, 79.
Warner, B. 1987, *MNRAS*, 227, 23.
Warner, B. 1995, *Cataclysmic Variable Stars* (Cambridge: Cambridge Univ. Press).
Whitehurst, R. 1988, *MNRAS*, 232, 35.
Wood, J.H., et al. 1989a, *ApJ*, 341, 974.
Wood, J.H., et al. 1989b, *MNRAS*, 239, 809.
Zola, S. 1989, *Acta Astr.*, 39, 45.

TABLE 1
LOG OF OBSERVATIONS

HJD Start (2,450,000+)	Length (hr)	Points	Telescope ^a	<V>	HJD Start (2,450,000+)	Length (hr)	Points	Telescope ^a	<V>
548.3791	4.76	189	1	14.04	565.6169	5.93	1276	11	16.88
548.5883	3.9	226	2	14.27	566.6156	5.86	1249	11	17.59
548.6145	7.2	334	3	14.3	567.5552	1.96	76	2	17.8
549.3785	4.96	150	1	14.25	567.7368	2.7	574	11	17.8
550.3219	0.27	11	1	14.1	1164.883	2.29	122	9	19.25
550.3145	5.52	160	4	14.2	1211.706	6.54	182	9	18.77
551.3138	4.93	138	4	14.65	1212.691	8.99	483	9	18.75
551.6926	4.79	250	3	14.66	1213.358	2.34	230	4	15.5
552.3256	0.5	18	1	14.6	1215.85	2.46	134	9	18.75
552.5376	2.59	128	2	14.54	1216.762	4.15	221	9	18.74
553.3104	5.15	152	4	14.68	1217.778	3.26	132	9	18.76
553.5421	4.5	282	2	14.72	1218.778	3.17	109	9	18.75
554.3034	6.12	175	4	15.06	1523.391	6.02	160	4	14.67
554.5239	4.94	313	2	14.97	1523.49	2.21	135	7	14.64
554.6254	6.89	343	3	14.91	1523.901	4.7	166	8	14.66
554.6745	4.81	181	10		1523.907	3.43	59	5	14.67
555.318	4.73	135	4	14.8	1526.374	3.74	96	4	14.99
556.3332	4.68	141	1	14.96	1526.783	5.59	80	5	15.03
557.3222	4.87	140	4	15.09	1529.368	1.08	39	7	15.13
558.3263	3.79	112	4	15.09	1531.46	4.73	106	4	15.49
560.3222	1.5	35	4	15.24	1531.724	6.52	1122	6	15.48
560.3494	2.88	47	1	15.02	1532.358	8.9	230	4	15.5
560.6565	3.88	881	11	14.99	1532.436	8.21	227	7	15.48
561.6212	4.51	967	11	15.1	1532.614	2.4	174	6	15.53
562.6231	4.38	928	11	15.7	1578.945	2.67	122	9	18.56
563.6119	4.64	932	11	15.7	1584.642	4.06	419	9	18.6
564.5635	2.97	156	2	15.9	1621.619	2.62	408	9	18.62
564.6127	4	840	11	16.05					

^aTelescope: 1 = CBA Belgium (0.25 m), 2 = CBA East (0.66 m), 3 = CBA West (0.35 m), 4 = CBA Denmark (0.25 m), 5 = CBA Alberta (0.41 m), 6 = CBA Alfred (0.81 m), 7 = CBA Belgium (0.35 m), 8 = CBA California (0.44 m), 9 = MDM (1.3 m), 10 = CBA Braeside (0.41 m), 11 = KPNO (0.9 m), 12 = MDM (2.4 m).

TABLE 2
TIMES OF ECLIPSE MINIMA

T_{\min} (HJD 2,450,000+)				
(548.3860)	552.5927	557.7441	566.6731	1526.9350
548.4727	553.3643	557.8295	566.8448	1531.4854
548.5570	553.4512	(558.3446)	567.7888	1531.7424
548.6440	553.6234	560.6630	949.6625	1531.8282
548.7310	553.7093	560.7491	1164.8951	1531.9140
548.8144	554.3945	561.6935	1211.8562	1532.6008
549.4180	554.4799	561.7798	1212.8861	1532.6867
549.5032	554.5672	562.6369	1523.4147	1578.9620
550.3609	554.6530	562.7227	1523.5007	1579.0480
550.4463	554.7393	563.6678	1523.5862	1584.7144
551.3894	554.8248	564.6984	1523.9299	1584.7999
551.4754	555.3394	565.6430	1524.0160	
551.7351	555.4252	565.7284	1526.5051	
551.8202	557.6584	565.8145	1526.8496	

TABLE 3
TIMINGS OF SUPERHUMP MAXIMA

(HJD 2,450,000+)					
548.427	550.410	552.633	554.678	558.399	563.701
548.514	550.500	553.344	554.768	560.687	563.789
548.605	551.390	553.434	554.856	560.784	564.670
548.689	551.481	553.612	555.383	561.672	564.762
548.780	551.749	554.323	555.473	561.759	565.619
548.858	551.844	554.413	557.691	562.643	566.660
549.447	552.368	554.507	557.780	562.730	566.749
549.533	552.540	554.588	557.867	563.612	566.832

TABLE 4
ECLIPSE MEASUREMENTS IN QUIESCENCE

t_{wdi}	t_{hsi}	t_{min}	t_{wde}	t_{hse}
(HJD 2,451,000+)				
164.89120		0.8951	0.89650	0.9000
211.		0.7705		
212.71102	0.71294	0.7145	0.71630	0.7201
212.79670	0.79902	0.8004	0.80220	0.8063
212.		0.8859	0.88815	0.8917
212.96902	0.97050	0.9718	0.97420	0.9774
213.05401	0.05650			
213.82715	0.8290	0.8307	0.83242	0.83605
215.		0.8908	0.89280	0.89620
216.91780		0.9209	0.92322	
584.71060	0.71250	0.7144	0.71589	0.71920
584.79627	0.79830	0.7999	0.80178	0.80528
578.95838	0.96010	0.9620	0.96395	0.96700
621.62713	0.62928	0.6315	0.63245	0.63615
658.71535	0.71742	0.7187	0.72065	0.72415
658.80115	0.80331	0.8050	0.80677	0.81000

FIGURE CAPTIONS

FIGURE 1. — O–C diagram of the eclipse timings, with respect to Eq. (1).

FIGURE 2. — *Upper left frame*, long light curve at quiescence, showing a double-humped waveform, a bright pre-eclipse hump arising from the “hot spot”, and deep eclipses. *Lower frames*, the mean orbital light curve in several passbands. *Upper right frame*, high-speed light curve through eclipse, superposed from two consecutive eclipses.

FIGURE 3. — The April 1997 superoutburst. Most of the filled squares are orbital averages from Table 1. Visual data collected in the VSNET archive have also been used to supplement these points, and to supply all the pre-outburst and post-outburst upper limits, which are indicated by open squares.

FIGURE 4. — Selected long light curves during superoutburst. The middle and lower frames show the “normal” features: deep eclipses plus powerful superhumps. The upper frame shows the first night of coverage, and the variation on that night appears to track the orbital period (see text).

FIGURE 5. — Cleaned amplitude spectrum of the JD 549–555 light curve, with the inset showing the mean superhump shape. Significant peaks are marked with their frequencies (± 0.01) in c/day. In superhump parlance, the marked peaks correspond in ascending frequency order to: $\omega - \Omega$, $2\omega - 2\Omega$, 2ω , $3\omega - 2\Omega$, $3\omega - \Omega$, and $4\omega - 4\Omega$, where ω and Ω are the orbital and “precession” frequencies. (Actually, the 2ω peak is probably present only during JD 548–9, as discussed in the text.)

FIGURE 6. — *Lower left frame*, O–C diagram of the superhump timings with respect to a test period of 0.0887 d. Most of the timings satisfactorily fit a simple parabolic ephemeris (Eq. 3), but the first night's data is highly discrepant and much better fit with the orbital period. *Upper frame*, power spectrum of the light curve during JD 548–9 only, with significant signals marked with their frequency in c/day (± 0.13). These are consistent with multiples of the orbital, not the superhump, frequency. *Lower right frame*, mean light curve of JD 548 folded on P_{orb} , showing a double-humped orbital variation cut off by eclipse.

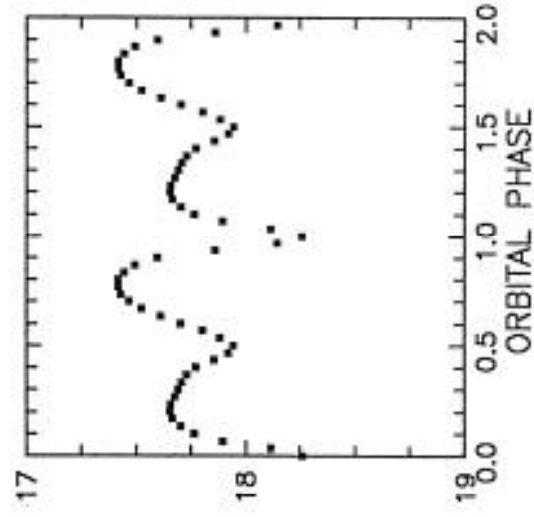
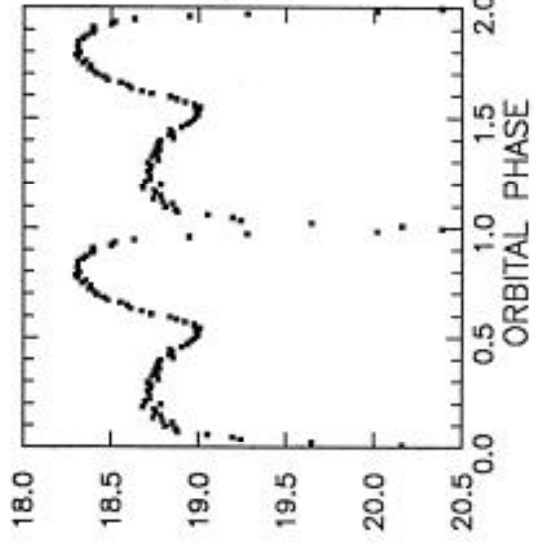
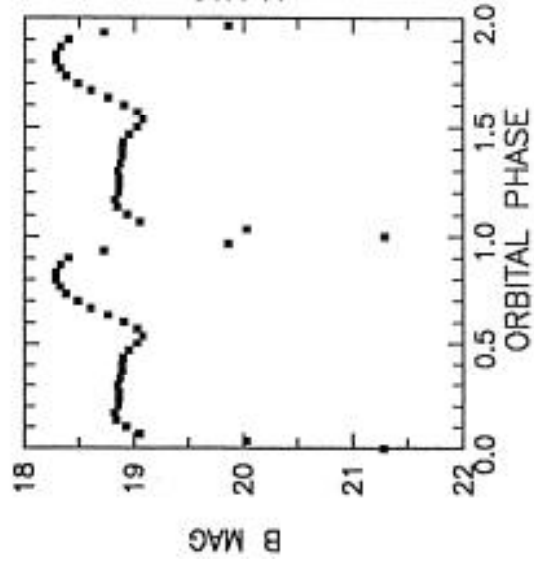
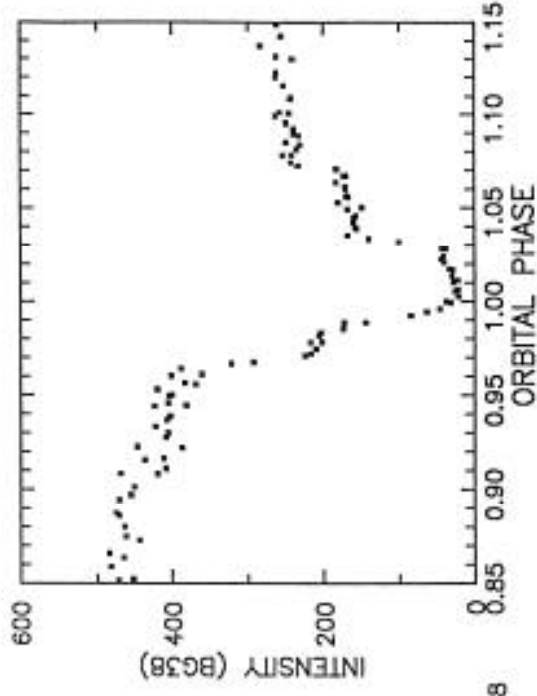
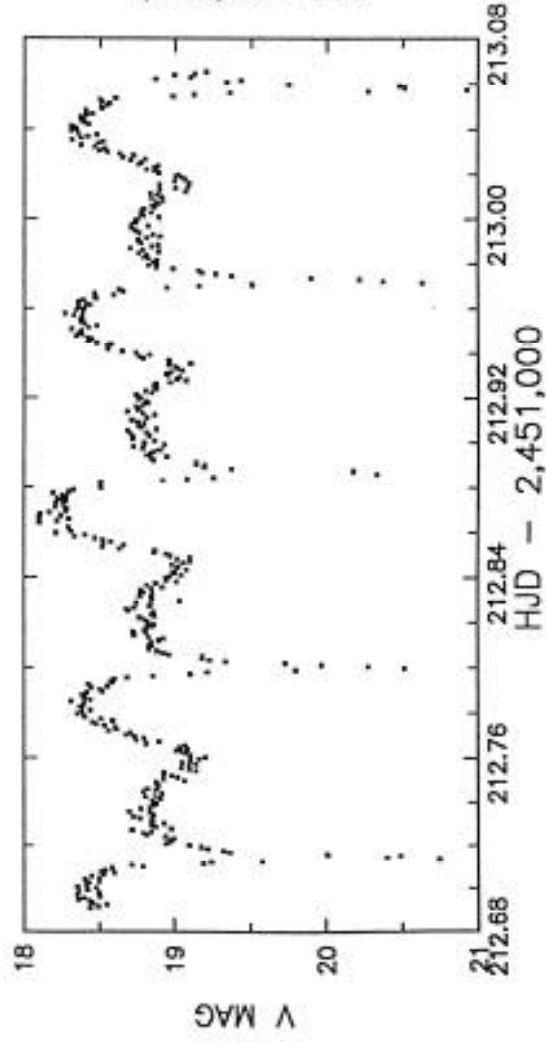
FIGURE 7. — *Lower frame*, power spectrum of the 1999 superoutburst light curves; significant signals are marked with their frequencies (± 0.01) in c/day, and the mean waveform is in the inset. The superhump was very similar to that of the 1997 eruption. *Upper left*, the visual history of the eruption. *Upper right*, O–C diagram of superhump timings with respect to a test period of 0.0887, showing a small period decrease.

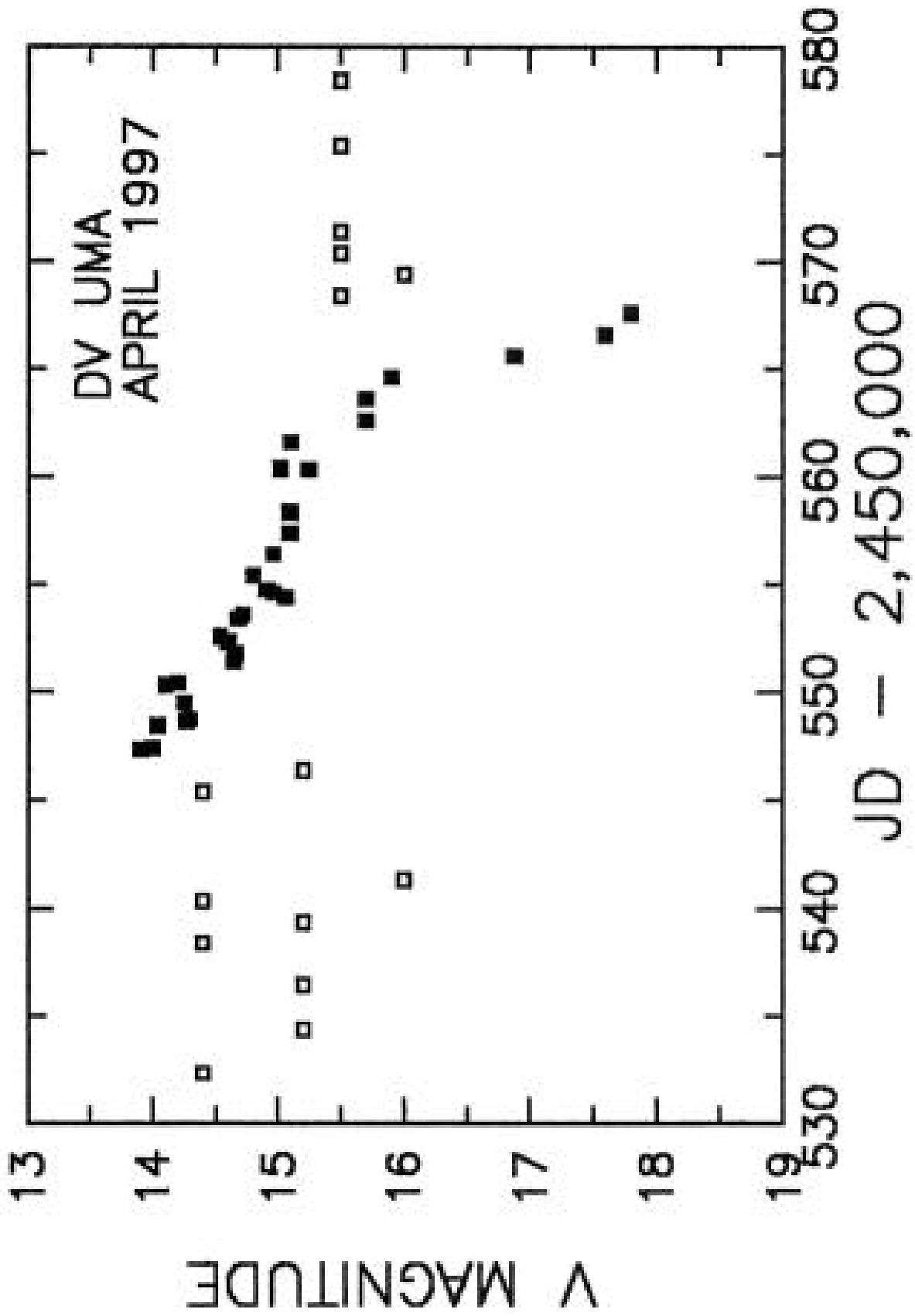
FIGURE 8. — Constraints on q and R_d/a from the eclipse timings in quiescence. We used average values (separately) from the 1999 and 2000 data. The curves are labeled with values of q , and the lines with values of R_d/a . We estimate $q = 0.155 \pm 0.015$.

FIGURE 9. — Eclipse constraints in the $M_2 - M_1$ plane. The eclipse width determines a $q(i)$

relation, and bounds on q are taken from the hot-spot eclipses studied in Figure 8. The hard limit at $i=90^\circ$ is also shown. The sides of the allowed region are set by the white dwarf eclipse duration, estimated as 30 ± 10 s. We slightly narrow this allowed (black) region with a constraint on the red star, discussed in the text.

FIGURE 10. — *Lower frame*, the variation of the full eclipse width W with time in the 1997 eruption. The inset scale shows corresponding values of R_d/a , but these estimates are much less reliable after JD 559, when the disk no longer dominated the light. *Upper frame*, the variation of superhump amplitude with time. Superhumps endure long after the disk shrinks within its 3:1 orbital resonance (which occurs at $R_d/a=0.46$). Representative error bars are shown in both frames.





NIGHTLY LIGHT CURVES OF DV UMA IN SUPEROUTBURST

